RSC Advances

ROYAL SOCIETY OF CHEMISTRY

www.rsc.org/advances

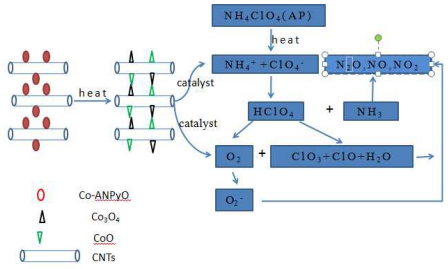

This research reported the preparation, characterization, thermal decomposition mechanism and catalytic performance of Co-ANPyO/CNTs nanocomposites.

Thermal Decomposition Mechanism of Co-ANPyO/CNTs Nanocomposites and Their Application To the Thermal Decomposition of Ammonium Perchlorate

Jian Cheng[1*], Rongxian Zhang[2], Zuliang Liu[3*], Lixia Li[1], Fengqi Zhao[4], Siyu Xu[4]

[1]School of Environment and Safety Engineering, Jiangsu University, Zhenjiang, Jiangsu 212013, P. R. China

[2]School of Chemistry and Chemical Engineering, Jiangsu University, Zhenjiang, Jiangsu 212013, P. R. China

[3]School of Chemical Engineering, Nanjing University of Science and Technology, Nanjing, jiangsu 210094, P. R. China

[4]Xi'an Modern Chemistry Research Institute, Xi'an, shanxi 710065, P. R. China

Corresponding author Tel.: +86 25 8431 8865; fax: +86 25 8431 5030.

E-mail address: chengjian09@foxmail.com(J. CHENG).

Abstract: Chemical precipitation method was used to prepare cobalt complex of 2,6-diamino-3,5-dinitropyridine-1-oxide/carbon nanotubes (Co-ANPyO/CNTs) nanocomposites. The structure and thermal analyses indicate that Co-ANPyO nanoparticles are well dispersed on the surface of CNTs with the average particle size about 10 nm, the content of Co-ANPyO nanoparticles in nanocomposites is about 73.4wt%. The thermal decomposition mechanism of Co-ANPyO and Co-ANPyO/CNTs nanocomposites were predicted base on thermogravimetry-differential scanning calorimetry (TG-DSC) and thermolysis in situ rapid-scan FTIR (RSFTIR) results. The thermal decomposition of Co-ANPyO and Co-ANPyO/CNTs nanocomposites contains two exothermic processes in the temperature range of 25-490 ^{o}C. The first exothermic process for Co-ANPyO/CNTs nanocomposites shifts towards lower temperature compared to that of Co-ANPyO.

And the main products of final residues for Co-ANPyO and Co-ANPyO/CNTs nanocomposites at 490 ^{o}C are Co_3O_4 and CoO, respectively. The catalytic performance of Co-ANPyO and Co-ANPyO/CNTs nanocomposites on thermal decomposition of ammonium perchlorate (AP) was investigated by TG-derivative thermogravimetry (DTG), DSC, non-isothermal kinetic and *α-T* kinetic curves analyses. And the possible catalytic mechanism was also discussed and proposed. During the thermal decomposition process of AP with Co-ANPyO/CNTs nanocomposites, Co-ANPyO/CNTs nanocomposites might decompose and form Co_3O_4/CNTs and CoO/CNTs nanocomposites as high activity catalysts, which could accelerate the thermal decomposition of AP. Thus, Co-ANPyO/CNTs nanocomposites not only lower the decomposition temperature and activation energy, but also enhance the total heat of AP, which could not be achieved by the CNTs and Co-ANPyO alone. The way of preparing Co-ANPyO/CNTs nanocomposites presented in this work can be expanded to other energetic additives/CNTs nanocomposites used for AP and AP based propellants.

Keyword: cobalt complex of ANPyO, CNTs, Co-ANPyO/CNTs nanocomposites, thermal decomposition mechanism, ammonium perchlorate, catalytic effect

As is well known, ammonium perchlorate (AP) is one of the most common oxidants in composite solid propellant, which has been used in various solid propellants. The thermal decomposition rate of AP-based propellant is related to the additives, which can influence the burning rate and pressure exponent of the propellant [1-3]. Considering its limitation in loading in composite solid propellant, it is important to improve decomposition efficiency of AP to satisfy the requirements of high energy generation at low burning temperature. Recent work has shown that nano-sized metals, metal oxides and complex oxides (such as Fe, Co, Ni, TiO_2, Co_3O_4, Fe_2O_3, ZnO, CuO, NiO, $LaCoO_3$ and $CuFe_2O_4$) exhibit high catalytic properties for AP thermal decomposition [4-16]. However, the disadvantages of these non-energetic additives is obvious, an increase in their concentration may decrease the total energy of the solid propellant, which is one of the most important performance parameters for

the solid propellant. In order to overcome these disadvantages, hunting for energetic additives with high catalytic activities is one of the future directions for the technology of AP thermal decomposition [17-22]. This possibly to be a hot research topic in both materials and chemistry fields [23-32].

Carbon nanotubes (CNTs) have attracted much attention from many researchers due to their superior mechanical, electrical and thermal properties [33-37]. In particular, their nano-scale size, low density, and high aspect ratio have put them into position as the promising candidate for reinforcement in composite materials. Recently, extensive attention has been paid on synthesis and characterization of nano-sized metals/CNTs and metal oxides/CNTs and their catalytic effects on thermal decomposition of 1,3,5-trinitrohexahydro-1,3,5-triazine (RDX) and AP [38-43]. These investigations show that the nano-size metals/CNTs and metal oxides/CNTs exhibit good catalytic effect on RDX and AP thermal decomposition, indicating metals/CNTs and metal oxides/CNTs nanocomposites can lead to a possible concerted effect or integration of the properties of the two components. However, energetic additives/CNTs nanocomposites have been investigated to a lesser extent than the other nanocomposites.

Inorganic 3d-transition cobalt compounds (Co, CoO, Co_3O_4, $CuCo_2O_4$, $CoC_2O_4{\cdot}2H_2O$) have attracted tremendous attention due to their remarkable catalytic effects on the thermal decomposition of AP [7, 8, 13, 24, 44, 45]. The reasons for these cobalt compounds such as CoO and Co_3O_4 exhibit remarkable catalytic performance for thermal decomposition of AP due to their high and stable catalytic activity and selectivity toward the oxidation of ammonia, the intermediate product of AP decomposition [8, 13, 44, 46]. Our early work reported the synthesis, crystal structure and properties of cobalt complex of 2,6-diamino-3,5-dinitropyridine-1-oxide (Co-ANPyO) [31]. Co-ANPyO is an insensitive, thermal stable energetic complex with a special coordination mode (Fig. 1), which has good compatibilities with RDX, cyclotetramethylene tetranitramine (HMX), nitrocellulose (NC) and aluminum (Al). Furthermore, differential scanning calorimetry (DSC) studies show that Co-ANPyO exhibits a good catalytic effect on the thermal decomposition of AP. However, the

thermal decomposition of AP catalyzed by Co-ANPyO has been studied, while the underlying mechanism of Co-ANPyO additives in the thermal decomposition of AP is not clear. More importantly, the aggregation of the Co-ANPyO particles in nature may result in its insignificant catalytic performance compared to that of nano-sized cobalt compounds [7, 8, 13, 24, 44, 45].

The purpose of this work is to improve the catalytic ability of Co-ANPyO additive in the thermal decomposition of AP, and investigate the mechanism of AP thermal decomposition catalyzed by Co-ANPyO. Thus, we developed a new strategy for the synthesis and characterization of Co-ANPyO/CNTs nanocomposites, and characterized with FTIR spectroscopy, scanning electron microscopy (SEM), transmission electron microscope (TEM), high-resolution scanning transmission electron microscopes (STEM), brunauer-emmett-teller (BET) and X-ray photoelectron spectroscopy (XPS). The thermal decomposition mechanism of Co-ANPyO and Co-ANPyO/CNTs nanocomposites was predicted base on thermogravimetry-differential scanning calorimetry (TG-DSC) and thermolysis in situ rapid-scan FTIR (RSFTIR) results. The catalytic performance of Co-ANPyO and Co-ANPyO/CNTs nanocomposites on the thermal decomposition of AP was investigated by TG-derivative thermogravimetry (DTG), DSC, non-isothermal kinetic and α-T kinetic curves analyses. The possible catalytic mechanism was also discussed and proposed.

2. Experimental

2.1. Materials and instrumentation

All chemicals used were analytical grade, and purchased from commercial sources without further purification. CNTs were purchased from commercial sources.

The FTIR studies were conducted with use of a Bruker (55FT-IR) FTIR Spectrometer (500-4000 cm^{-1}). Elemental contents of carbon, hydrogen, and nitrogen were determined by a German Vario EL III analyzer. SEM images were obtained on JEM-2000CX scanning electron microscope. An H-8100 TEM operating at 200 kV accelerating voltage was used for TEM. XPS was performed with an American Thermo ESCALAB 250 electron spectrometer using Al K irradiction. DSC analyses

were recorded on a TA-DSC-Q20 from 25 to 500 ^{o}C, TG-DTG analyses were conducted on a TGA/SDTA851eMETTLER TOLEDO from 25 to 500 ^{o}C. The detailed microscopic structure and the chemical composition of the Co-ANPyO/CNTs nanocomposites were investigated using high-resolution scanning transmission electron microscopes (Cs-corrected HR-STEM, JEM2010F and JEM2200FS operating at 200 kV, JEOL).

The conditions of TG-DTG and DSC were: sample mass, about 1.2-1.5 mg; N_2 flowing rate, 40 cm^3min^{-1}; heating rates (β), 2.5, 5, 10 and 15 ^{o}C/min, furnace pressures, 0.1 MPa; reference sample, α-$A1_2O_3$; type of crucible, aluminum pan with a pierced lid.

RSFTIR measurements were conducted using a Nicolet Model NEXUS 870 FT-IR Instrument and in situ thermolysis cell (Xiamen University, China) in the temperature range of 20-500 ^{o}C. Ar flowing rate, 10 cm^3min^{-1}. Heating rate: 10 ^{o}C/min. KBr pellet samples, well mixed by about 1.5 mg samples and 120 mg KBr were used. Infrared spectra in the range of 4000-500 cm^{-1} were obtained by model DTGS detector at a rate of 15 files min^{-1} and 10 scans $file^{-1}$ with 5 cm^{-1} resolution.

2.2. Synthesis and preparation

2.2.1 Synthesis of ANPyO

ANPyO was prepared according to the literature [31]. Anal. Calcd.(%):C, 27.89; H, 2.32; N, 32.54. Found: C, 27.87; H, 2.35; N, 32.52.

2.2.2 Synthesis of Co-ANPyO

Co-ANPyO was prepared according to the literature and recrystallized by N,N-dimethyl-Formamide (DMF) [31]. Anal. Calcd.(%):C, 23.84; H, 2.38; N, 27.82. Found: C, 23.85; H, 2.39; N, 27.81. IR, (KBr, cm^{-1}):3608, 3418, 3382, 3298, 3060, 1602, 1536, 1458, 1380, 1314, 1236, 1173, 1124, 1050, 951, 810, 744, 695, 620, 568.

2.2.3 Synthesis of Co-ANPyO/CNTs nanocomposites

Co-ANPyO/CNTs nanocomposites were prepared by chemical precipitation method, the synthesis process was described as follows:

Preparation of ANPyO solution: ANPyO (0.5 g, 2.3 mmol) was dissolved in DMF (60 ml) at 120 ^{o}C for 60 min, and kept the temperature of the solution at 60-70

^{o}C for the next step.

Preparation of Co-ANPyO/CNTs nanocomposites: CNTs (0.5 g), tetrabutyl ammonium bromide (0.12 g) and $Co(NO_3)_2 \cdot 6H_2O$（0.65 g，2.3 mmol）were added in distilled water (300 ml) under ultrasound condition at 70 ^{o}C for 45 min, subsequently, the ANPyO solution was added into the above mixture stirring at 80 ^{o}C drop by drop, after that, the solution was stirred at 80 ^{o}C under ultrasound condition for another 2.5 h. Finally, the sample was collected by filtration, washed with distilled water several times, dried and heated at 50 ^{o}C for 7 h.

2.2.4 Preparation of Co-ANPyO/CNTs/AP and Co-ANPyO/AP mixtures

The Co-ANPyO/CNTs/AP and Co-ANPyO/AP mixtures were prepared by dry mixed. The content of the Co-ANPyO and Co-ANPyO/CNTs nanocomposites in AP was 5wt%.

3 Results and Discussion

3.1 Characterizations

Fig. 2(a) shows the SEM image of Co-ANPyO, in which the samples of Co-ANPyO were recrystallizied by DMF. The shape of the samples is cuboid and smooth, with the average particle size and specific surface area of about 12 um and 0.96 m^2/g. The SEM image of CNTs (Fig. 2(b)) shows that most of the CNTs in the arrays appear to slightly tangle or curved, and these tube roots are isolated and have almost same diameter (about 50 nm), no particles are observed. Fig. 2(c) shows the TEM image of Co-ANPyO/CNTs nanocomposites, in which clearly discloses that there are no obvious changes in the morphology of CNTs, most of the CNTs in the TEM image almost keep the original state. However, it can be seen clearly that there are a lot of small Co-ANPyO nanoparticles uniformly deposited on the surface of CNTs, with the average particle size about 10 nm. The Co-ANPyO nanoparticles are anchored tightly and well dispersed on the surface of CNTs, forming compact coating, and the individual Co-ANPyO nanoparticles are well separated from each other. The growth of newborn Co-ANPyO nanoparticles is depressed due to the intense friction and collisions of the molecules created by ultrasound condition. With ultrasound condition of reactant in DMF and water, temperature and concentration gradients

could be avoided, providing a uniform environment for the nucleation and growth of Co-ANPyO nanoparticles [47]. Furthermore, CNTs sheet could inhibit the aggregation of Co-ANPyO nanoparticles [48-49]. This helps to prevent Co-ANPyO nanoparticles from agglomerating and guarantee the efficient catalytic activities of the Co-ANPyO/CNTs nanocomposites.

STEM image and elemental mapping analysis of Co-ANPyO/CNTs nanocomposites (Fig. 2(d-h)) also suggest the presence of Co, C, N and O components in the Co-ANPyO/CNTs nanocomposites, which indicate that there are a lot of small Co-ANPyO nanoparticles uniformly deposited on the surface of CNTs.

The FTIR spectrum is used to further confirm the functional groups of CNTs, Co-ANPyO and Co-ANPyO/CNTs nanocomposites, respectively, as shown in Fig. 3. As can be seen in Fig. 3(a), the FTIR spectrum of CNTs discloses the presence of 1650(C=C) and 2090(C=C) cm^{-1}, which are in agreement with the functional groups of CNTs. As can be seen in Fig. 3(b), the FTIR spectrum of Co-ANPyO discloses the presence of 3608(H_2O), 3420(NH_2), 3337(NH), 3298(NH_2), 3064, 1124, 810, 744, 695(CH), 1583(NH, NH_2), 1524(C=C, C=N), 1458(NO_2), 1374(NO_2), 1308(N-O), 568(Co-N) and 620(Co-O) cm^{-1}, respectively, which are in agreement with the functional groups of Co-ANPyO [31]. And the FTIR spectrum of Co-ANPyO/CNTs nanocomposites (Fig. 3(c)) shows that the characteristic peaks for CNTs and Co-ANPyO could be determined in the FTIR, while the intensity of the characteristic peaks for CNTs and Co-ANPyO turn to be weaken, maybe caused by the fine loading of Co-ANPyO nanoparticles on CNTs surface.

By XPS measurement of the CNTs, Co-ANPyO and Co-ANPyO/CNTs nanocomposites (Fig. 4), the chemical composition of Co-ANPyO/CNTs nanocomposites can be further confirmed. As shown in Fig. 4(a), in which discloses the presence of C and O for CNTs, respectively. C 1s XPS spectrum of CNTs in Fig. 4(b) shows four types of carbon with different chemical states are observed, in which appear at 284.3(C-C), 284.9(C-OH), 287.2(C=O) and 290.5 ev(COOH), respectively [50]. It is noted that the C/O ratio for CNTS in the composite is estimated to be 93:7, which indicates some degree of oxidation with three components that correspond to

carbon atoms in different functional groups.

For the case of Co-ANPyO in Fig. 4(a), in which discloses the presence of C, N, O and Co, respectively. XPS spectrum of Co-ANPyO also exhibits two peaks at 781.1 and 796.0 eV, corresponding to $Co2p_{3/2}$ and $Co2p_{1/2}$ spin-orbit of Co-ANPyO, respectively, which confirm the formation of cobalt [8]. The presence cobalt can be further confirmed by Co 2p, N 1s and O 1s XPS spectrums of Co-ANPyO in Fig. 4(c), Fig. 4(d) and Fig. 4(e), respectively, in which the characteristic peaks close to 780.5($Co2p_{3/2}$), 795.7($Co2p_{1/2}$), 397.4 (Co-N) and 530.5 (Co-O) ev. This confirms the formation of Co-N and Co-O bonds in the molecular structure of Co-ANPyO. As can be seen in Fig. 4(b), C 1s XPS spectrum of Co-ANPyO shows four types of carbon with different chemical states are observed, which appear at 283.1(C-H), 284.2(C=C), 285.0(C-N) and 286.6 ev(C=N), respectively. Fig. 4(d) and Fig. 4(e) also exhibit the N 1s and O 1s XPS spectrums of Co-ANPyO, six types of nitrogen and four types of oxygen with different chemical states are observed, in which appear at 397.4(N-Co), 398.7(N-H), 400.4(N-C), 401.1(N=C), 404.1(N-O, N→O), 405.9(N-O, NO_2), 530.5(O-Co), 531.2(O-H, H_2O), 532.0(O-N, N→O) and 533.7 ev(O-N, NO_2), respectively.

For the case of Co-ANPyO/CNTs nanocomposites in Fig. 4(a), in which discloses the presence of C, N, O and Co, respectively. The C 1s, N 1s, Co2p and O 1s XPS spectrums of Co-ANPyO/CNTs nanocomposites in Fig. 4 indicate that there are no obvious changes in the chemical states for N1s and Co2p, but some changes for C1s and O1s. The C 1s and O 1s XPS spectrums of Co-ANPyO/CNTs nanocomposites disclose that the content of C-C, C-OH, C=O and COOH groups significant increase compared to that of Co-ANPyO. The XPS results prove that the nanoparticles of Co-ANPyO are formed and load on the CNTs surface.

BET analyses are performed to further investigate the specific surface area of the nanoparticles, which is one of most important factors that guarantee the efficient catalytic activities of catalyst. As shown in Fig. 5, the Co-ANPyO/CNTs

nanocomposites show a type H3 hysteresis loop in the range of P/P_o with the specific surface area of 43.1 m^2/g, in which is higher than that of normal-sized Co-ANPyO (<1.0 m^2/g).

Base on SEM, TEM, STEM, FTIR, XPS and BET Characterizations for CNTs, Co-ANPyO and Co-ANPyO/CNTs nanocomposites, we conclude that the Co-ANPyO nanoparticles are formed and well dispersed on the surface of CNTs in the chemical precipitation process. On the basis of our experimental results, a scheme has been presented to describe such a formation process of Co-ANPyO/CNTs nanocomposite, as illustrated in Fig. 6.

3.2 Thermal decomposition mechanism of Co-ANPyO and Co-ANPyO/CNTs

In order to realize the thermal decomposition mechanism of Co-ANPyO and Co-ANPyO/CNTs, thermal decomposition of CNTs, Co-ANPyO and Co-ANPyO/CNTs was investigated by TG-DSC and RSFTIR measurements at the heating rate of 10 ^oC/min, the results were shown in Fig. 7 and Fig. 8, respectively.

3.2.1 Thermal decomposition of CNTs

As is well known, CNTs have good thermal and chemical stability, which are considered as good support for catalyst [37]. As shown in Fig. 7, there are no obvious changes in the TG-DSC curves for CNTs in the range of 25-500 ^oC, in which reveal that CNTs do not decompose during this process. Thus, we hypothesis that CNTs in Co-ANPyO/CNTs nanocomposites do not decompose during the heating process in the range of 25-500 ^oC.

3.2.2 Thermal decomposition mechanism of Co-ANPyO

The FTIR spectrum of Co-ANPyO at room temperature is shown in Fig. 3(b). The stretching vibration absorption of $V_{(C\text{-}NO2)}$ peaks are at 1458 and 1374 cm^{-1} for the NO_2, the $V_{(NH2)}$ peaks are at 3420, 3298 and 1583 cm^{-1} for the NH_2, the $V_{(CH)}$ peaks are at 3064, 1124, 810, 744 and 695 cm^{-1} for C-H, the $V_{(NH)}$ peak is at 3337 cm^{-1} for the NH, the $V_{(OH)}$ peak is at 3608 cm^{-1} for the H_2O, the $V_{(NO)}$ peak is at 1308 cm^{-1} for the N→O, the $V_{(Co\text{-}N)}$ peak is at 568 cm^{-1} for the C_O-N and the $V_{(Co\text{-}O)}$ peak is at 620 cm^{-1} for the C_O-O.

As can be seen in Fig. 8, the absorption peak of H_2O almost disappears at 200 ^oC, while the other characteristic groups do not change. Corresponding to the TG-DSC curves, there is a mass loss of 7.0% in this process, which corresponds well with the calculation value of 7.1%, while no obvious changes from the DSC curve. This process would be the loss of three H_2O molecules from the Co-ANPyO.

The first exothermic stage for the Co-ANPyO occurs in the range of 250.0-303.9 ^oC with the peak temperature at 287.8 ^oC. Corresponding to this process, there is a mass loss of 33.1% from the TG curve. It can be seen that the absorption peaks of NH_2 and NO_2 decrease, and the absorption peaks of C-H, N→O, Co-O and Co-N almost disappear. Furthermore, the new absorption peaks at 665, 548, 460 and 430 cm^{-1} prove the existence of Co_3O_4 and CoO in the solid residue [44, 51]. This process would be the Co-O, Co-N bonds breaking of the Co-ANPyO and the ring breaking of the ligands, which may be attributed to the partial decomposition of Co-ANPyO.

The second exothermic stage occurs in the range of 303.9-380.3 ^oC with the peak temperature at 315.0 ^oC. Corresponding to this process, there is a mass loss of 16.9% from the TG curve. The cleavage of the amino-groups and nitro-groups can be confirmed by the disappearance of the absorption bands of $V_{(NH2)}$, $V_{(C\text{-}NO2)}$ and $V_{(NH)}$, respectively. The breaking of the pyridine ring can be confirmed by the disappearance of the absorption bands of $V_{(C\text{-}H)}$, $V_{(N\rightarrow O)}$, $V_{(C=C)}$ and $V_{(C=N),}$ respectively. While the new absorption peaks at 665, 548, 460 and 430 cm^{-1} for Co_3O_4 and CoO keep increasing. The other new absorption peak at 2165 cm^{-1} prove the existence of $Co(NCO)_2$ in the solid residue [52]. But the intensity of $Co(NCO)_2$ is weaker compared to that of Co_3O_4 and CoO, which implies that $Co(NCO)_2$ might be the by-product for solid residue. This process would be the O-Co, N-Co bonds breaking of the Co-ANPyO and the ring breaking of the ligands, which may be attributed to the completely decomposition of Co-ANPyO.

On the TG curve, there still is a slow mass loss of 3.1% from 380.3 to 490 ^oC. Corresponding to this process, there are no obvious changes from DSC and RSFTIR curves. Therefore, the decomposition pathway of Co-ANPyO may be described as follows:

$$Co(C_5H_4N_5O_5)_3.3H_2O \xrightarrow{200\ ^oC} Co(C_5H_4N_5O_5)_3 + 3H_2O$$

$$\xrightarrow{400\ ^oC} Co_3O_4 + CoO + Co(NCO)_2(\text{by-product}) + \text{gas products}$$

3.2.3 Thermal decomposition mechanism of Co-ANPyO/CNTs

As can be seen in Fig. 7, there are no obvious difference in the thermal decomposition behaviors for Co-ANPyO and Co-ANPyO/CNTs nanocomposites, but some changes in decomposition pattern. The first exothermic stage of Co-ANPyO/CNTs nanocomposites occurs in the range of 138.7-278.6 ^oC with the peak temperature at 248.1 ^oC, which notably shifts towards lower temperatures compared to that of Co-ANPyO. However, there are no obvious changes in the second exothermic stage of Co-ANPyO/CNTs nanocomposites compared to that of Co-ANPyO. Nano-size particles exhibit an increase in the ratio of surface atoms to interior atoms compared to that of normal-size particles [53]. This may lead to a higher surface energy and result in the decrease of the temperature for thermal decomposition process. This is the main reasons for above phenomenon. Furthermore, the absorption peaks at 2165, 665, 548, 460 and 430 cm^{-1} also prove the existence of Co_3O_4, CoO and $Co(NCO)_2$ in the solid residue at 490 ^oC, which are in agreement with that of Co-ANPyO. According to the mass loss of Co-ANPyO and Co-ANPyO/CNTs nanocomposites, about 73.4wt% of Co-ANPyO deposited on the surface of CNTs.

Base on above results, we propose that the main solid products for thermal decomposition of Co-ANPyO and Co-ANPyO/CNTs nanocomposites are Co_3O_4 and CoO, respectively, which may be contributed to the catalytic effects of AP thermal decomposition.

3.3 Catalytic effects of Co-ANPyO and Co-ANPyO/CNTs nanocomposites on the thermal decomposition of AP

3.3.1 Thermal decomposition of pure AP, Co-ANPyO/AP and Co-ANPyO/CNTs/AP

Recently, the thermal decomposition of AP catalyzed by CNTs has been investigated by Liu [54]. This investigation shows that CNTs exhibits insignificant catalytic effects on the thermal decomposition of AP.

TG, DTG and DSC results of the decomposition of AP, Co-ANPyO/AP and Co-ANPyO/CNTs/AP were shown in Fig. 9 and Table 1, respectively. As shown in Fig. 9(a), the DSC curve for pure AP reveals that the thermal decomposition of AP takes place in three steps: the endothermic phase transition at 242.3 ^{o}C (ascribed to a phase transition of AP from orthorhombic to cubic), the low-temperature decomposition (LTD) at 332.2 ^{o}C and the high-temperature decomposition (HTD) at 432.5 ^{o}C (contributed to intermediate products such as NH_3 and $HC1O_4$ and a complete one to volatile products respectively) [55]. Corresponding, the TG, DTG curves for pure AP reveal that the 20wt% weight loss at LTD is attributed to the partial decomposition of AP. The 75wt% weight loss at HTD is attributed to the complete decomposition of the intermediate to volatile products [55].

When Co-ANPyO is added, the DSC result for Co-ANPyO/AP reveals that the HTD process crakes into two steps, and the LTD and HTD processes shift towards lower temperatures compared to that of pure AP. Corresponding, the TG, DTG curves for Co-ANPyO/AP reveal that there are 11.0wt% weight loss at LTD process and 89.0wt% weight loss at HTD process. This shows that the LTD process for Co-ANPyO/AP is narrowed down, while the HTD process for Co-ANPyO/AP is enlarged. The overall heat for HTD and LTD processes (1084 J/g) is 429 J/g, which is higher than that of pure AP. The TG, DTG and DSC curves of Co-ANPyO/AP show that Co-ANPyO additive has no effects on the crystallographic transition temperature, but some changes in the decomposition pattern. AP decomposition is accelerated in the presence of the Co-ANPyO.

The TG, DTG and DSC results for Co-ANPyO/CNTs/AP show a difference thermal decomposition behavior compared to that of pure AP and Co-ANPyO/AP. Typically, the HTD process for Co-ANPyO/CNTs/AP disappeared, while the LTD for Co-ANPyO/CNTs/AP shows a peak temperature closer to that observed for pure AP, but higher than that of Co-ANPyO/AP. This indicates that Co-ANPyO/CNTs

nanocomposites do not influence the primary dissociation of AP into ammonia and perchloric acid, but most likely catalyze the secondary process involved in AP decomposition, and accelerates the overall decomposition process. Similar effects have been found from nano-sized Co, CoO, Co_3O_4, $CuCo_2O_4$, $CoC_2O_4{\cdot}2H_2O$, but have not been discussed in detail [7, 8, 13, 24, 45, 56]. This indicates a difference catalytic mechanism for Co-ANPyO and Co-ANPyO/CNTs nanocomposites. The LTD process for the mixture systems (337.8 ^oC) is 94.7 ^oC, which is lower than HTD of pure AP. And decomposition heat of 1850 J/g is observed in the presence of Co-ANPyO/CNTs nanocomposites, nearly triple the decomposition heat for pure AP.

Base on above results, it show that both of CNTs and Co-ANPyO exhibit insignificant catalytic effects on the thermal decomposition of AP. However, because of the combination of the CNTs and Co-ANPyO for the catalysis of AP decomposition, Co-ANPyO/CNTs nanocomposites not only lower the decomposition temperature, but also enhance the total heat of AP, which could not be achieved by the CNTs and Co-ANPyO alone. Furthermore, a lot of research on the decomposition of AP catalyzed by cobalt compounds (such as Co, CoO, Co_3O_4, $CuCo_2O_4$, $CoC_2O_4{\cdot}2H_2O$, Co-ANPyO) and nanocomposites (such as Co_3O_4/grapheme oxide, Co_3O_4/CNTs) has been carried out [7, 8, 13, 24, 31, 45, 56, 57-59]. And some of these cobalt catalysts can decrease exothermic peaks of LTD and HTD processes for AP to slightly lower temperature than that of Co-ANPyO/CNTs nanocomposites. While this work shows that AP with Co-ANPyO/CNTs nanocomposites shows notably higher decomposition heat than that of AP with all of these cobalt catalyst, which suggests better catalytic effect than these cobalt catalysts.

3.3.2 Nonisothermal reaction kinetics of pure AP, Co-ANPyO/AP and Co-ANPyO/CNTs/AP

DSC and kinetic parameters of the overall decomposition processes for pure AP, Co-ANPyO/AP and Co-ANPyO/CNTs/AP, estimated by the Kissinger's method, were given in Table 2 [60]. A decrease in the apparent activation energy (E_a) of LTD and HTD processes for Co-ANPyO/AP are observed in the catalysed systems. Similar situation in the E_a of LTD process for Co-ANPyO/CNTs/AP is observed, but exhibits

higher E_a than that of LTD process for Co-ANPyO/AP. The E_a of LTD and HTD processes for AP decomposition, associates with the primary dissociation step and completely decomposition step [61]. The above results indicate that Co-ANPyO not only influences the primary dissociation of AP, but also influences the completely decomposition of AP. While Co-ANPyO/CNTs nanocomposites do not influence the primary dissociation of AP, which is in agreement with the TG-DTG and DSC results.

It can be seen that both of Co-ANPyO/CNTs nanocomposites and Co-ANPyO increase the overall heat for HTD and LTD processes of AP. In general, Co-ANPyO/CNTs nanocomposites exhibit higher catalytic activity than that of Co-ANPyO.

3.3.3 *α-T* kinetic curves of pure AP, Co-ANPyO/AP and Co-ANPyO/CNTs/AP

To explore the thermal decomposition mechanism of pure AP, Co-ANPyO/AP and Co-ANPyO/CNTs/AP, the corresponding *α-T* (α is the extent of conversion, $0<\alpha<100$) kinetic curves (Fig. 10) were obtained by dealing the TG curves and compared. It has been shown that the thermal decomposition of Co-ANPyO/AP starts at lower temperatures than that of pure AP. This temperature difference points toward the AP decomposition catalyzed by Co-ANPyO.

However, It can be seen from the figure that, during the stages decomposition ($\alpha<10$), the thermal decomposition of Co-ANPyO/CNTs/AP starts at higher temperatures than that of pure AP and Co-ANPyO/AP for the same extent of conversion. While during the stages decomposition ($10<\alpha<95$), the thermal decomposition of Co-ANPyO/CNTs/AP shows significantly lower temperature than that of pure AP and Co-ANPyO/AP for the same extent of conversion. This indicates a difference catalytic mechanism for AP catalyzed by Co-ANPyO and Co-ANPyO/CNTs nanocomposites, which is in agreement with the TG, DTG, DSC and Nonisothermal reaction kinetics results.

By means of *α-T* kinetic curves investigation, Co-ANPyO/CNTs nanocomposites exhibit higher catalytic activity than that of Co-ANPyO.

3.4 Possible catalytic mechanism of Co-ANPyO and Co-ANPyO/CNTs on the thermal decomposition of AP

Based on above experimental results, we conclude that Co-ANPyO/CNTs nanocomposites play better catalytic role than that of Co-ANPyO on AP thermal decomposition. TG, DTG, DSC, non-isothermal kinetic and α-T kinetic curves analyses indicate that Co-ANPyO/CNTs nanocomposites do not influence the primary dissociation of AP into ammonia and perchloric acid, but most likely catalyze the secondary process involved in AP decomposition. While Co-ANPyO influences both the LTD and HTD processes for AP decomposition. What is reason for this phenomenon?

We have proposed that (**3.2**) the main solid products for thermal decomposition of Co-ANPyO and Co-ANPyO/CNTs nanocomposites are Co_3O_4 and CoO, respectively. AP decomposition involves two crucial steps: (1) ammonia oxidation and (2) dissociation of ClO_4^- species into ClO_3^- and O_2 [46]. In the first step, Co_3O_4 and CoO exhibit high and stable catalytic activity and selectivity toward ammonia oxidation, thus promoting the partial decomposition of AP [46]. In the second step, Co_3O_4 and CoO belong to p-type semiconductor, which could release of O^{2-} ions, form easy melting eutectics or intermediate amine compounds with AP, thus promoting the completely decomposition of AP[62]. According to proton transfer mechanism, it can be proposed that the Co-ANPyO decomposes and releases a large amount of heat itself. This enhances the total heat of the AP mixture, as well as the formation of Co_3O_4 and CoO in situ on the AP surface. Therefore, the Co_3O_4 and CoO used here can speed up above two controlling steps [56, 63].

For the case of Co-ANPyO/CNTs nanocomposites, CNTs exhibits some catalytic effects on the thermal decomposition of AP [54]. And we have concluded that the thermal decomposition process for Co-ANPyO/CNTs nanocomposites shifts towards lower temperature compared to that of Co-ANPyO (**3.2**). Thus, this might result in formation Co_3O_4/CNTs and CoO/CNTs nanocomposites in situ at lower temperatures. More importantly, CNTs sheet could inhibit the aggregation of the Co_3O_4 and CoO nanoparticles. We hypothesize that CNTs is more likely to aggregate and expose active sites to absorb ammonia which covers the CNTs surface, then create a supersaturated atmosphere of NH_3 [64-65]. This might result in depriving the catalytic

activities of Co_3O_4/CNTs and CoO/CNTs nanocomposites. As a result, the LTD process Co-ANPyO/CNT/AP shifts towards relatively higher temperature. As the temperature rises, the catalytic activities of Co_3O_4/CNTs and CoO/CNTs nanocomposites recover, the ammonia would be oxidized with a higher speed catalyzed by Co_3O_4/CNTs and CoO/CNTs nanocomposites. And the completely decomposition of AP would be accelerated with a higher speed catalyzed by Co_3O_4/CNTs and CoO/CNTs nanocomposites.

A possible mechanism of AP thermal decomposition catalyzed by Co-ANPyO/CNTs nanocomposites is proposed, as shown in Fig. 11.

4. Conclusion

Co-ANPyO nanoparticles were obtained by chemical precipitation method using CNTs, $Co(NO_3)_2 \cdot 6H_2O$ and ANPyO as raw materials. The Co-ANPyO nanoparticles are well dispersed on the surface of CNTs with the average particle size about 10 nm, the content of Co-ANPyO nanoparticles in nanocomposites is about 73.4wt%. Thermal analyses show that the thermal decomposition of Co-ANPyO and Co-ANPyO/CNTs nanocomposites contains two exothermic processes in the temperature range of 25-490 ^oC. The main products of final residues for them at 490 ^oC are Co_3O_4 and CoO, respectively. TG, DTG, DSC, non-isothermal kinetic and α-T kinetic curves investigations show that Co-ANPyO/CNTs nanocomposites not only lower the decomposition temperature, but also enhance the total heat of AP, which could not be achieved by the CNTs and Co-ANPyO alone. The way of preparing Co-ANPyO/CNTs nanocomposites presented in this work can be expanded to other energetic additives/CNTs nanocomposites used for AP and AP based propellants.

Acknowledgements

We gratefully acknowledge the financial support from Nanjing University of Science and Technology and Xi'an Modern Chemistry Research Institute. This work is supported by Five-Year (2011-2015) Pre-research Project (NO.62201070102).

Reference

1 S. Vyazovkin and C. A. Wight, *Chem Mater*., 1999, **11**, 3386.

2 L. Bereczk, K. Marthi and P. Huszthy, *J Therm Anal Calorim*., 2004, **78**, 449.

3 H. Xu, X. Wang and L. Zhang, *Powder Technol*., 2008, **185**, 176.

4 A. Dey, J. Athar and P. Varma, *RSC Adv*., 2015, **5**, 1950.

5 X. F. Guan, L. P. Li and J. Zheng, *RSC Adv*., 2011, **1**, 1808.

6 D. L. Reid, A. E. Russo and R. V. Carro, *Nano Lett*., 2007, **7**, 2157.

7 H. Y. Zhao, L. Guo and S. F. Chen, *RSC Adv*., 2013, **3**, 19929.

8 S. S. Liu, X. Y. Jing and J. Y. Liu, *J Solid State Chem*., 2013, **197**, 345.

9 Z. Ma, F. Li and H. Bai, *Propel Explos Pyrot*., 2006, **31**, 447.

10 X. Sun, X. Qiu and L. Li, *Inorg Chem*., 2008, **47**, 4146.

11 J. Yin, Q. Lu and Z. Yu, *Crys Growth & Des*., 2009, **10**, 40.

12 J. Zhu, G. Zeng and F. D. Nie, *Nanoscale*., 2010, **2**, 988.

13 J. Wang, Z. Q. Qiao and L. Zhang, *CrystEngComm*., 2014, **16**, 8673.

14 L. J. Chen, G. S. Li and P. Qi, *J Therm Anal Calorim*., 2008, **92**, 765.

15 Y. P. Wang, X. J. Yang and L. D. Lu, *Powder Technol*., 2008, **185**, 231.

16 T. Liu, L. S. Wang and P. Yang, *Mater Lett*., 2008, **62**, 4056.

17 G. Singh and S. P. Felix, *Combust Flame*., 2003, **132**, 422.

18 Z. Cheng, G. Zhang and X. Fan, *Inorg Chim Acta*., 2014, **421**, 191.

19 Q. Li, Y. He and R. F. Peng, *RSC Adv*., 2015, **5**, 24507.

20 Q. Yang, S. Chen and G. Xie, *J Hazard Mater*., 2011, **197**, 199.

21 M. Friedrich, J. C. Gálvez-Ruiz and T. M. Klapötke, *Inorg Chem*., 2005, **44**, 8044.

22 D. E. Jones, K. Armstrong and T. Parekunnel, *J Therm Anal Calorim*., 2006, **86**, 641.

23 R. P. Singh, R. D. Verma and D. T. Meshri, *Angew Chem Int Edit*., 2006, **45**, 3584.

24 M. Zou, X. H. Jiang and L. D. Lu, *J Hazard.Mater*., 2012, **225**, 124.

25 N. Li, M. H. Cao and Q. Y. Wu, *CrystEngComm*., 2012, **14**, 428.

26 K. Karaghiosoff, T. M. Klapotke and P. Mayer, *Inorg Chem*., 2008, **47**, 1007.

27 H. B. Liu, Q. Z. Jiao and Y. Zhao, *J Alloy Comp*., 2010, **496**, 317.

28 M. Kaiser, U. Ticmanis and A. Hammerl, *Inorg Chem*., 2001, **40**, 3570.

29 Y. Shvedenkov, M. Bushuev and G. Romanenko, *Eur J Inorg Chem*., 2005, **167**, 1678.

30 J. J. Liu, Z. L. Liu and J. Cheng, *J Solid State Chem*., 2013, **197**, 198.

31 J. J. Liu, Z. L. Liu and J. Cheng, *RSC Adv*., 2013, **3**, 2917.

32 J. J. Liu, Z. L. Liu and J. Cheng, *J Solid State Chem*., 2013, **200**, 43.

33 P. M. Ajayan and J. M. Tour, *Nature*., 2007, **447**, 1066.

34 R. H. Baughman, A. A. Zakhidov and W. A. Heer, *Science*., 2002, **297**, 787.

35 T. W. Ebbesen, H. J. Lezec and H Hiura, *Nature*., 1996, **382**, 54.

36 P. Kim, L. Shi and A. Majumdar, *Phys Rev Lett*., 2001, **87**, 2155021.

37 M. F. Yu, O. Lourie and M. J. Dyer, *Science*., 2000, **287**, 636.

38 X. J. Zhang, W. Jiang and D. Song, *Mater Lett*., 2008, **62**, 2343.

39 H. Ren, Y. Liu and Q. Jiao, *J Phys Chem Solids*., 2010, **71**, 149.

40 P. Cui, and A. Wang, *J Saudi Chem Soc*., 2014., in press.

41 P. Cui, F. Li and Z. Jian, *Propell Explos Pyrotech*., 2006, **31**, 452.

42 X. Zhang, W. Jiang and D. Song, *Propell Explos Pyrotech*., 2009, **34**, 151.

43 M. Zheng, Z. Wang and J. Wu, *Nanopart Res*., 2010, **12**, 2211.

44 E. Santacesaria, A. Morini and S. Carra, *Combust Flame*., 1978, **31**,17.

45 E. Alizadeh-Gheshlaghi, B. Shaabani and B. Shaabani, *Powder Technolo*., 2012, **217**, 330.

46 (a) Y. Matatov-Meytal and M. Sheintuch, *Ind Eng Chem Res*., 1998, **37**, 309. (b) K. Schmidt-Szalowski, K. Krawczyk and J. Petryk, *Appl Catal A*., 1998, **175**, 147.

47 H. Zhu, C. Zhang and Y. Yin, *J Crys Growth*., 2004, **270**, 722.

48 W. X. Chen, J. Y. Lee and Z. Liu, *Mater Lett*., 2004, **58**, 3166.

49 R. Licheri, R. Orrù and C. Musa, *Mater Lett*., 2008, **62**, 432.

50 V. Datsyuk, M. Kalyva and K. Papagelis, *Carbon*., 2008, **46**, 833.

51 N. N. Binitha, P. V. Suraja and Z. Yaakob, *J Sol-Gel Sci Technol*., 2010, **53**, 466.

52 T. B. Brill and T. L. Zhang, *Combust Flame*., 2000, **121**, 662.

53 B. Gao, P. Wu and B. Huang, *New J Chem*., 2014, **38**, 2334.

54 J. Liu, W. Jiang and Z. Wang, *Acta Chim Sin-chin Edit*., 2007, **65**, 2725.

55 L. Song, S. Zhang and B. Chen, *Colloids Suf A*., 2010, **360**, 1.

56 L. P. Li, X. F. Sun and X. Q. Qiu, *Inorg Chem*., 2008, **47**, 8839.

57 C. Xu, X. Wang and J. Zhu, *J Mater Chem*., 2008, **18**, 5625.

58 J. Zhao, Z. S. Liu and Y. L. Qin, *CrystEngComm*, 2014, **16**, 2001.

59 J. X. Liu, F. S. Li and W. Jiang, *J Solid Rocket Tech*., 2007, **30**, 243.

60 H. E. Kissinger, *Anal Chem*., 1957, **29**, 1702.

61 R. A. Chandru, S. Patra and C. Oommen, *J Mater Chem*., 2012, **22**, 6536.

62 S. A. Makhlouf, *J Magn Magn Mater*., 2002, **246**, 184.

63 G. Singh, I. P. S. Kapoor and S. H. Dubeyl, *J Sci Confer Proceed*., 2009, **1**, 11.

64 P. W. M. Jacobs and A. Russell-Jones, *AIAA J*., 1967, **5**, 829.

65 S. S. Joshi, P. R. Paul and V. I. V. Krishnamurthy, *AIAA J*., 2008, **58**, 721

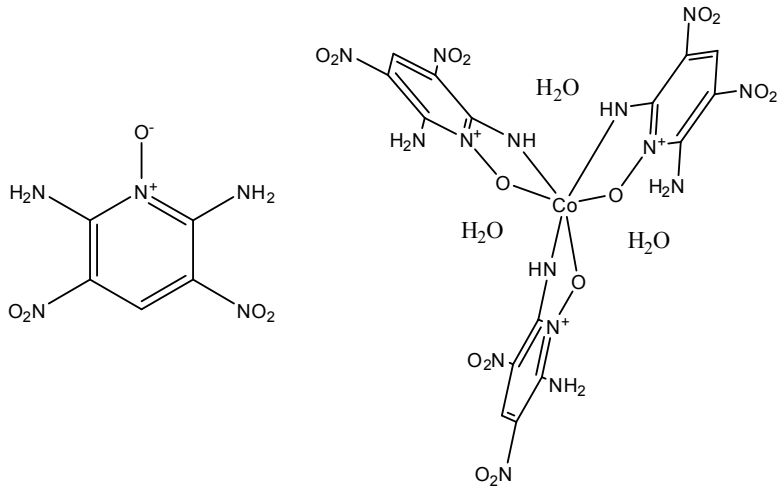

(a) (b)

Fig.1 Molecular structures of ANPyO (a) and Co-ANPyO (b)

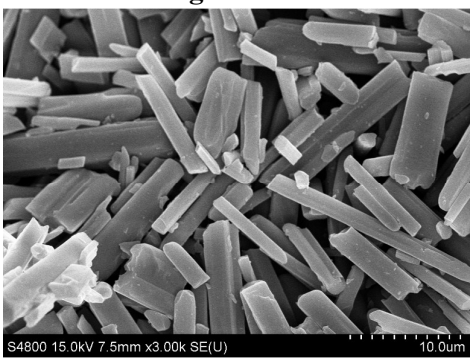

(a)

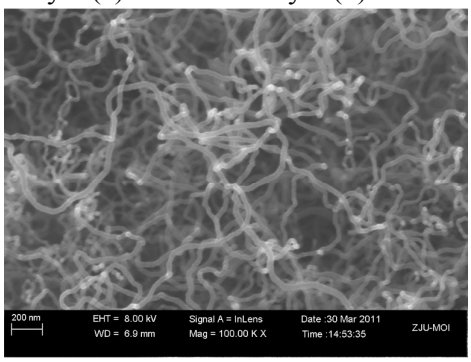

(b)

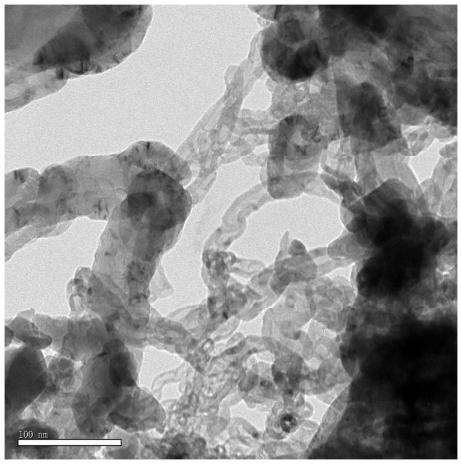

(c)

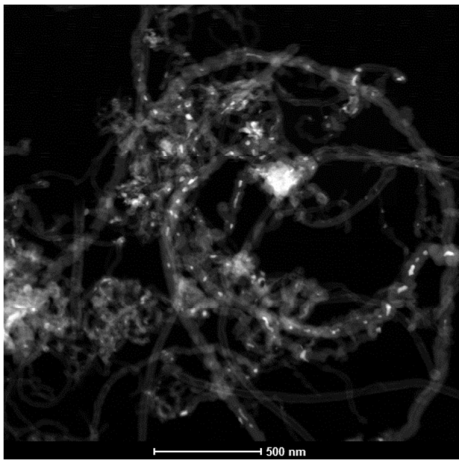

(d)

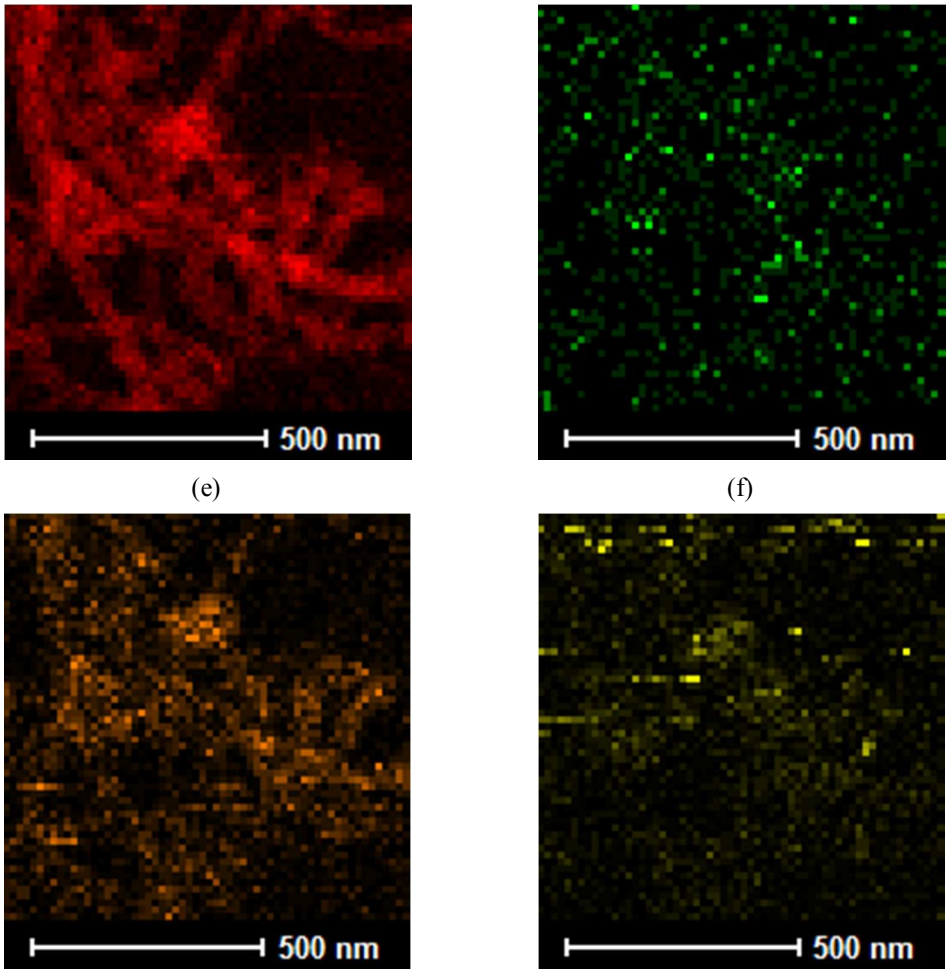

Fig. 2 SEM images of Co-ANPyO (a), CNTs (b), TEM, STEM images of Co-ANPyO/CNTs nanocomposites (c-d) and corresponding elemental mapping images of C, Co, N, O (e-h)

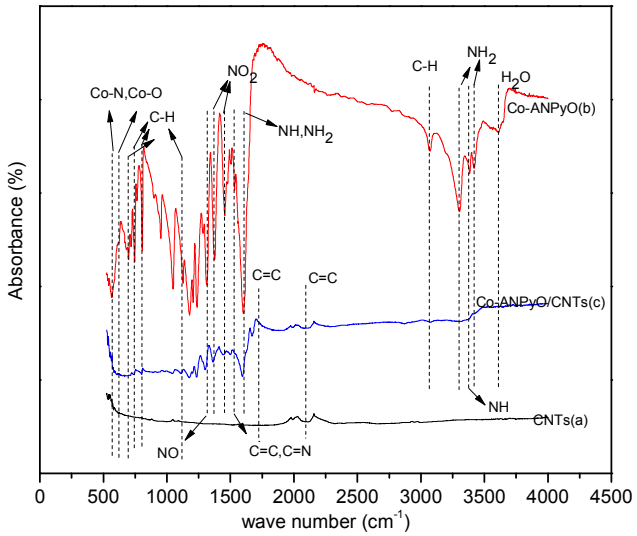

Fig. 3 FTIR spectrums of pristine CNTs, Co-ANPyO and Co-ANPyO/CNTs

nanocomposites

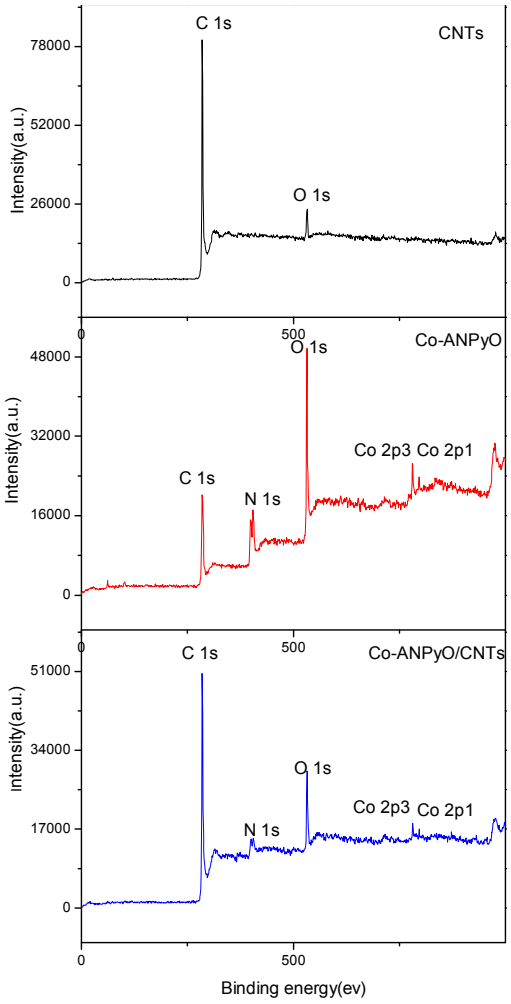

(a)

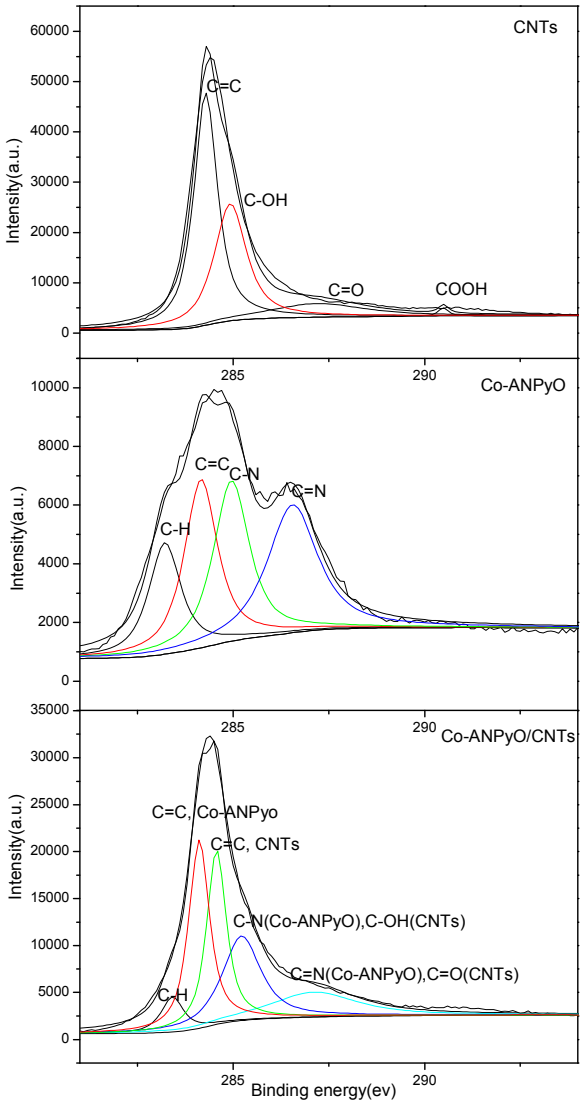

(b)

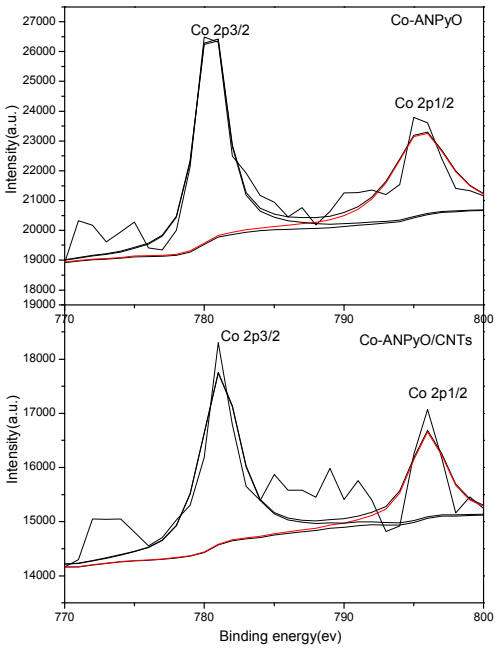

(c)

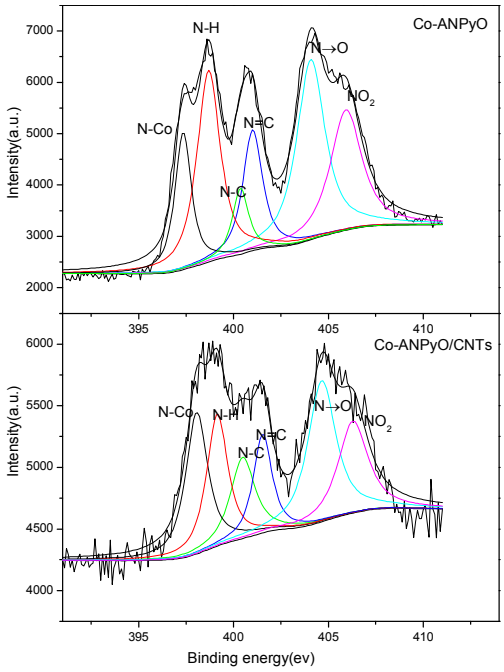

(d)

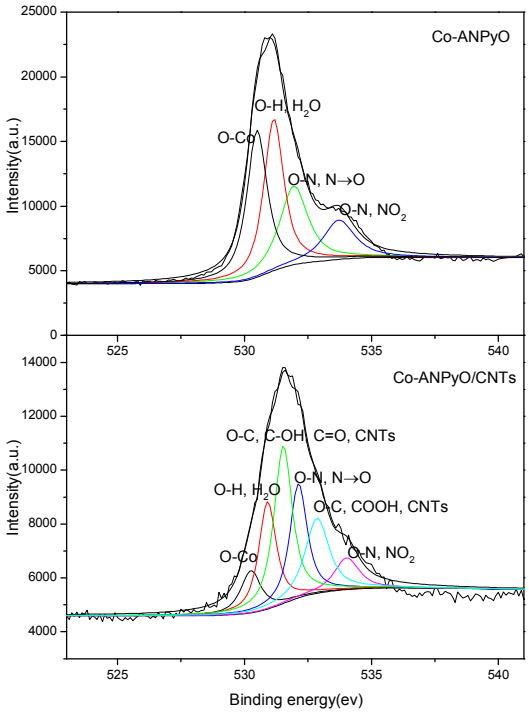

(e)

Fig. 4 XPS patterns of Co-ANPyO/CNTs nanocomposites, Co-ANPyO and CNTs(a), C 1s XPS spectrums of Co-ANPyO/CNTs nanocomposites, Co-ANPyO and CNTs (b), Co 2p XPS spectrums of Co-ANPyO/CNTs nanocomposites and Co-ANPyO (c) N 1s XPS spectrums of Co-ANPyO/CNTs nanocomposites and Co-ANPyO (d) and O 1s XPS spectrums of Co-ANPyO/CNTs nanocomposites and

Co-ANPyO

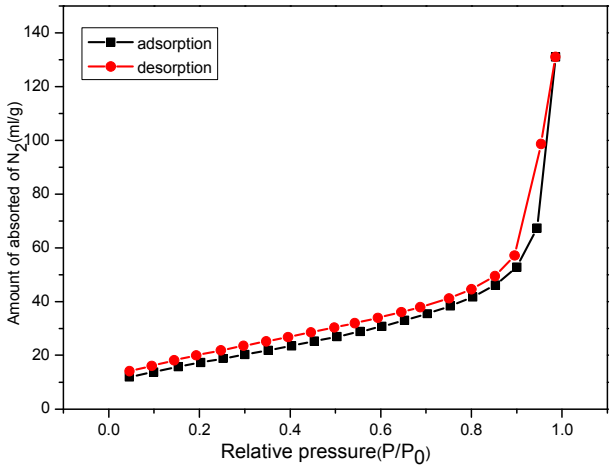

Fig. 5 Nitrogen adsorption-desorption isotherms for Co-ANPyO/CNTs nanocomposites

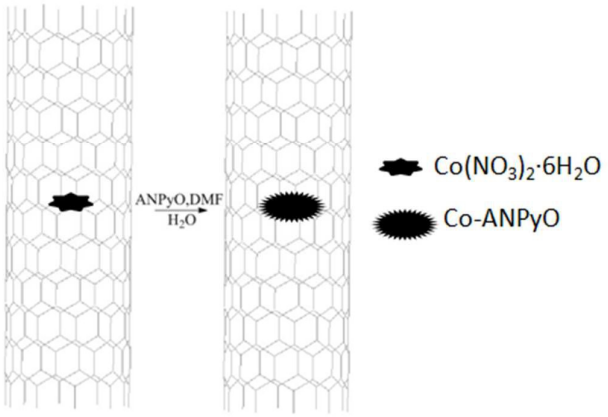

Fig. 6 A scheme shows a proposed formation route of Co-ANPyO nanoparticles onto the surfaces of CNTs sheets

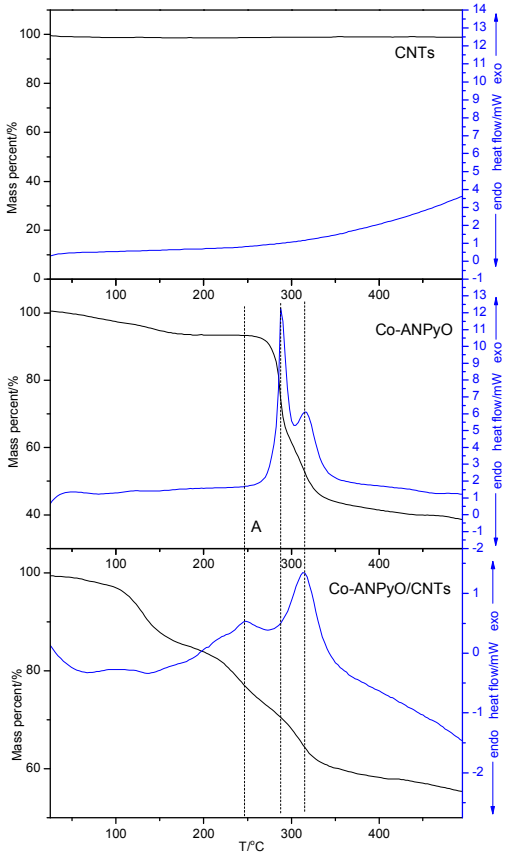

Fig. 7 TG-DSC curves of Co-ANPyO and Co-ANPyO/CNTs nanocomposites at the heating rate of 10 °C/min

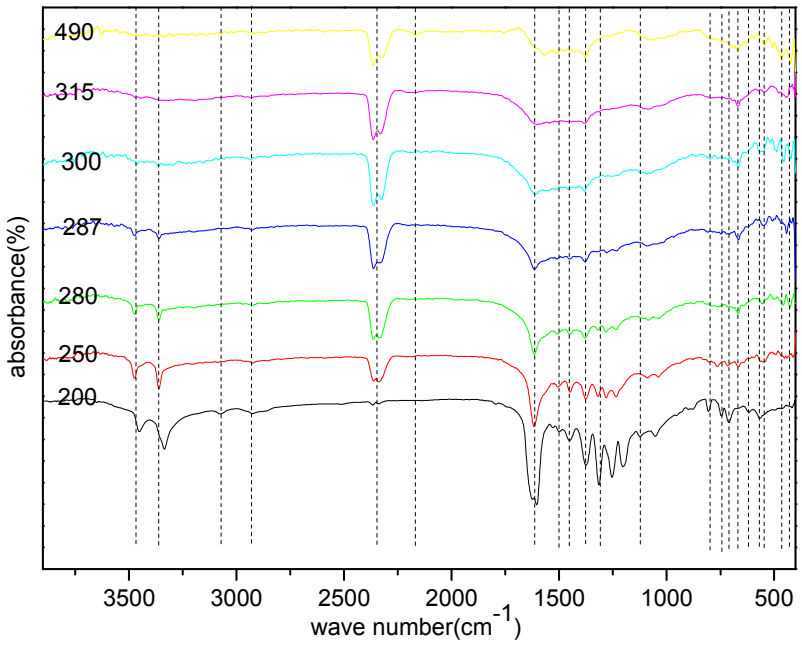

Fig. 8 The RSFTIR spectrums of Co-ANPyO at different temperatures

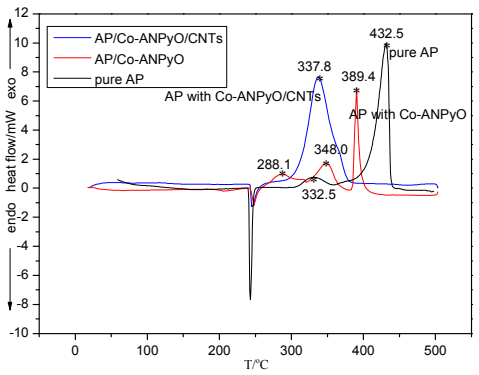

(a)

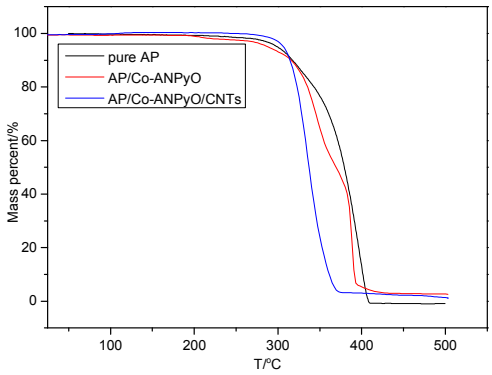

(b)

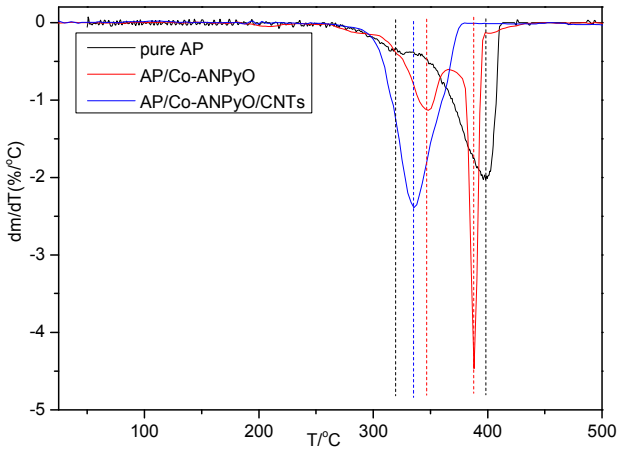

(c)

Fig. 9 TG, DTG and DSC curves for AP, Co-ANPyO/AP and Co-ANPyO/CNTs/AP at the heating rate of 10 °C /min

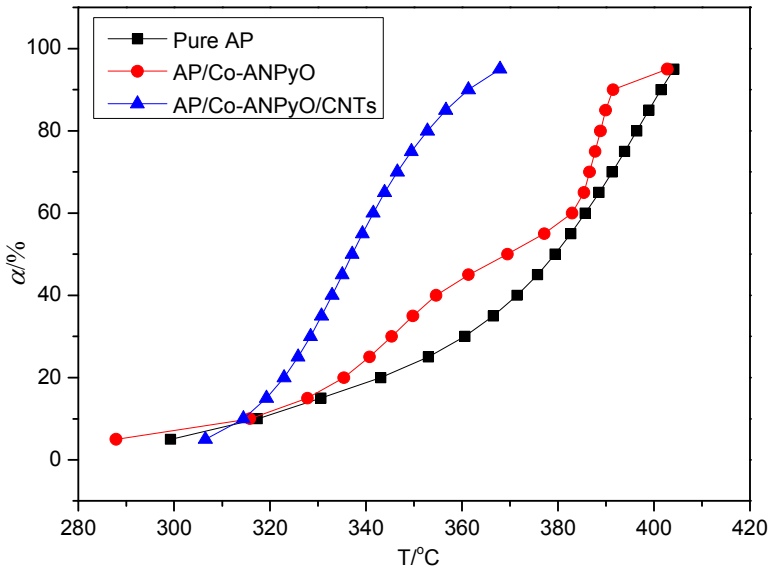

Fig. 10 *α-T* kinetic curves for AP, Co-ANPyO/AP and Co-ANPyO/CNTs/AP at the heating rate of 10 °C/min

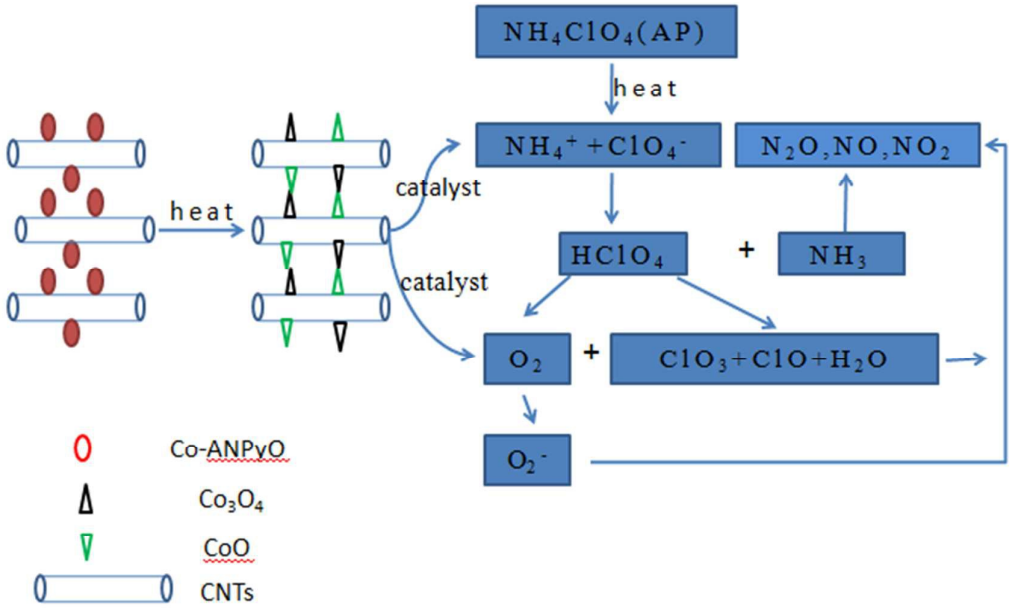

Fig.11 Mechanism of AP thermal decomposition catalyzed by Co-ANPyO/CNTs nanocomposites

Table 1 TG-DTG and DSC results for pure AP, Co-ANPyO/AP and Co-ANPyO/CNTs/AP additives in LTD and HTD processes

sample	endothermic peak/°C	LTD				HTD				ΔH/J/g
		T_o/°C	T_p/°C	T_e/°C	Mass loss/%	T_o/°C	T_p/°C	T_e/°C	Mass loss/%	
Pure AP	242.3	304.3	332.2	353.9	20	363.1	432.5	443.6	75	655
Co-ANPyO/AP	246.8	256.5	288.1	321.0	11	321.0, 382.7	348.0, 389.4	382.7, 426.5	49,40	1084
Co-ANPyO/CNTs/AP	245.1	282.8	337.8	383.4	100	-	-	-	-	1850

Note: T_o, onset temperature of decomposition for DSC curve. T_e, end temperature of decomposition for DSC curve. T_p, peak temperature of decomposition for DSC curve.

Table 2 Summary of DSC and Kinetic parameters results for pure AP, Co-ANPyO/AP and Co-ANPyO/CNTs/AP additives in LTD and HTD processes

sample	β/(°C·min^{-1})	ΔH/J/g	LTD			HTD		
			T_p/°C	E_a/(kJ/mol)	R^2	T_p/°C	E_a/(kJ/mol)	R^2
Pure AP	2.5	208	310.9	173.9	0.9975	405.5	185.6	0.9895
	5	244	321.5			421.2		
	10	655	332.2			432.5		
	15	689	340.2			443.1		
Co-ANPyO/AP	2.5	855	263.5	139.7	0 .9855	313.5, 342.7	158.5, 90.47	0.9781, 0.9901
	5	1039	273.7			328.6, 366.8		
	10	1084	288.1			339.8, 386.5		
	15	1221	292.5			345.2, 405.7		
Co-ANPyO/CNTs/AP	2.5	1767	310.8	148.5	0.9765	-	-	-
	5	1833	320.6			-		
	10	1850	337.6			-		
	15	1897	342.6			-		